optica

Thin film wavelength converters for photonic integrated circuits

Lin Chang,[1,*] Yifei Li,[1] Nicolas Volet,[1] Leiran Wang,[1,2] Jon Peters,[1] and John E. Bowers[1]

[1]Department of Electrical and Computer Engineering, University of California, Santa Barbara, California 93106, USA
[2]State Key Laboratory of Transient Optics and Photonics, Xi'an Institute of Optics and Precision Mechanics, Chinese Academy of Sciences, Xi'an 710119, China
*Corresponding author: linchang@ece.ucsb.edu

Quasi-phase-matched (QPM) wavelength converters are highly desirable for emerging nonlinear optics applications in photonic integrated circuits, but available waveguide and quasi-phase-matching technologies have so far constrained their realization. In this work, we present a periodically poled lithium niobate (LN) waveguide on a silicon nitride–thin film LN platform. It contains a submicrometer waveguide core for enhancing nonlinear interactions that is more than one order of magnitude smaller than those of previous QPM waveguides. Periodic poling was applied directly to the thin film LN for quasi-phase-matching by a new surface poling technology. We demonstrated $160\% \; W^{-1} \cdot cm^{-2}$ normalized efficiency for second harmonic generation at 1530 nm with ultralow propagation loss (0.3 dB/cm) in the telecom band. This highly efficient and compact wavelength converter has the potential for straightforward integration with various photonic platforms, e.g., on-chip microsystems such as optical communication networks, quantum storage, and optical frequency referencing.   © 2016 Optical Society of America

OCIS codes: (160.3730) Lithium niobate; (190.2620) Harmonic generation and mixing; (190.4390) Nonlinear optics, integrated optics.

http://dx.doi.org/10.1364/OPTICA.3.000531

1. INTRODUCTION

Highly efficient, compact, and integration compatible wavelength converters using quasi-phase-matched (QPM) optical waveguides are crucial for merging integrated nonlinear optics microsystems in optical communication networks [1], quantum storage [2], and optical frequency references [3,4]. However, efforts to develop such QPM waveguide in photonic integrated circuits (PICs) have been unsuccessful [5–8], mainly due to the difficulties in fabricating waveguides of nonlinear materials and the small size domain inversion for quasi-phase-matching. Among all existing QPM wavelength converters, the periodically poled lithium niobate (PPLN) waveguide is the most widely used because lithium niobate (LN) has a broad transparent window (350 nm to 4.5 μm) and large nonlinear coefficients [9]. Optical waveguides on LN are commonly fabricated either with titanium (Ti) indiffusion [5,6] or with proton exchange [10,11]. Both methods suffer from weak optical confinement, resulting in a large optical mode size. In addition, the waveguide modes at different wavelengths have poor overlap due to the weak asymmetric gradient-index profile [10]. This significantly reduces the wavelength conversion efficiency. Other LN waveguide approaches, such as etching and mechanical structuring, have also been investigated [12–14]. However, etching LN often results in rough waveguide sidewalls, leading to large optical loss, especially for submicrometer dimensions. Additionally, mechanical structuring is not suitable for fabricating narrow waveguides. Prior to this work, the smallest

mode size in a PPLN waveguide device [15] was larger than 10 μm². Poling the LN is another challenge, since usually, a bulk z-cut wafer was required and only worked for TM polarization. This is incompatible with most of the on-chip applications [1–4]. In contrast, surface poling applied on an x-cut (or y-cut) LN wafer [16,17] works for TE polarization. However, its poling depth (~1 μm) is too small for the optical modes of the conventional LN waveguide [16]. Surface poling is also challenging, since the random domain growth and leakage currents can result in poor poling quality [18]. Due to these problems, previously reported PPLN devices have large-scale, low conversion efficiencies and are incompatible with photonic integration.

In this work, we present the first QPM waveguide device compatible with PICs: a PPLN wavelength converter on a silicon nitride (SiN) thin-film LN platform. This approach can be used to fabricate LN waveguides with submicrometer dimensions. Due to the high index contrast of the waveguide structure, the optical mode is tightly confined. The mode overlap issue of the previous waveguide PPLN devices is eliminated, as the optical mode distributions for different wavelengths are similar in this waveguide structure. These two advantages significantly enhance the nonlinear interaction. For the first time, periodical poling is successfully realized on an LN thin film with a new surface poling technique that eliminates the aforementioned surface-poling quality issues. This method is designed for TE polarization and allows fabricating an ultra-short poling period (shorter than 2.4 μm in our experiment).

2. FABRICATION

Figure 1 shows the processing flow for the fabrication of a PPLN wavelength converter. The fabrication of devices is based on a commercial LNOI substrate wafer (supplied by NANOLN). The LNOI wafer consists of a 700-nm-thick x-cut LN film and a 2-μm-thick buried SiO_2 layer on an LN substrate. Two lift-off processes are used to deposit the poling electrodes; these are made of chrome (Cr) and gold (Au). The first lift-off process defines the electrode teeth and the contact pads. A bottom 30-nm-thick Cr layer is in direct contact with the LN film, and a top 40-nm-thick Au layer protects the Cr from oxidation. In the second lift-off process, an extra 1-μm-thick Au layer is deposited on the contact pads. This lowers the electric resistance and improves the uniformity of the poling voltage over the PPLN device. The spacing between the electrodes is 20 μm, and the poling period is 6.6 μm. The contact pads, which define the periodically poled region, are 4.8 mm long.

After electrode deposition, surface poling is done, during which the sample is placed in a silicone oil bath to prevent air breakdown under a high voltage. Contact electrode pads are connected to a voltage source by two electrical probes (Wentworth PVX400). Electrodes are removed by wet etching after poling. A 390-nm-thick SiN layer is then deposited on the LN by sputtering. Inductively coupled plasma then partially etches this layer to form a 2-μm-wide and 5-mm-long ridge waveguide. The etching depth is ~350 nm. Finally, a 1-μm-thick SiO_2 layer is deposited by sputtering to form the waveguide top cladding.

As every step of fabrication is performed on the LN film without the limitations of substrates, this method is compatible with a variety of integration platforms [e.g., Si, SiN, silicon oxynitride (SiON)] where the LN film is integrated with different material systems via wafer bonding [19–22].

The device cross section is schematized in Fig. 2(a): an SiN ridge is defined on top of an x-cut LN thin film to form the waveguide. As SiN has a slightly smaller refractive index (1.98) than LN (2.13 for extraordinary rays at 1550 nm), it can laterally guide the optical mode and leave most of the power in the LN core, which is suitable for nonlinear interaction. In addition, because SiN has a broad transparency range, the waveguide loss can be kept low over a spectral range broader than any other existing heterogeneous LN waveguide platforms [19–21]. Figures 2(c) and 2(d) depict the simulated TE waveguide mode profile at the fundamental (1550 nm) and the second harmonic generation (SHG) (775 nm) signals, respectively, simulated with
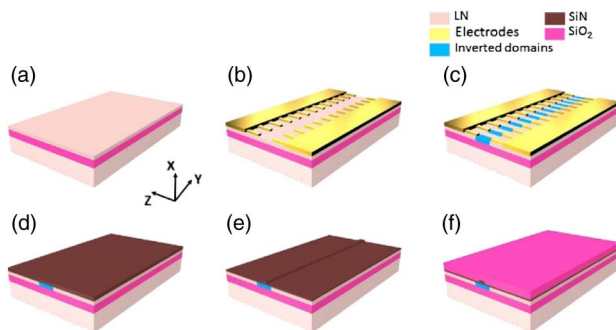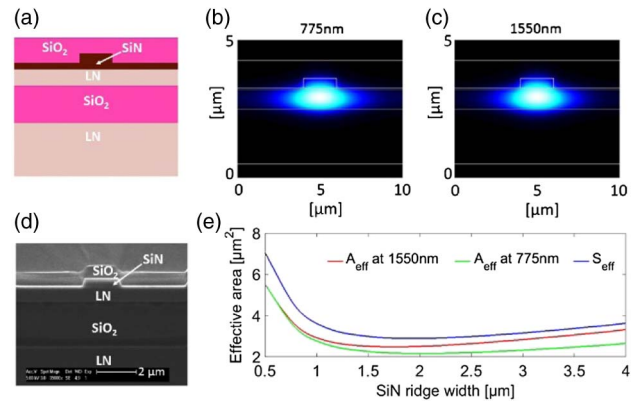

Fig. 2. Waveguide structure and simulation: (a) schematic cross section of the device; (b) SEM image taken after the sample is polished and then dipped in BHF for 1 min to improve the contrast; (c) and (d) simulated fundamental TE mode profiles of the waveguide at 1550 and 775 nm, respectively; and (e) simulated effective waveguide area (A_{eff}) for the fundamental TE mode at 775 and 1550 nm, and S_{eff} between these two modes as a function of the SiN ridge width.

FIMMWAVE [23]. Due to the high index contrast structure (~0.6) and the submicrometer thickness of the LN film, the waveguide modes are confined into an area that is more than one order of magnitude smaller than that obtained with proton exchange or with Ti in-diffusion [10]. This directly relates to more than an extra order of magnitude improvement for the efficiency of nonlinear effects (see Supplement 1). For both modes, over 90% of the power is confined in the LN film.

As depicted in Fig. 2(e), by tailoring the size of the SiN ridge, the optical mode cross sections A_{eff} at both the telecom band (1550 nm) and the corresponding second harmonic light (775 nm) can be reduced to around 2 μm^2. Also, the effective area of S_{eff} between these two modes for SHG (see Supplement 1) is close to the effective waveguide areas for both wavelengths, suggesting good overlap. This is also critical for achieving high conversion efficiency.

Due to the small mode size of this SiN-LN waveguide, the waveguide geometry creates significant dispersion. Therefore, in order to achieve quasi-phase-matching, a short poling period of ~6.6 μm is required for a 1530 nm working wavelength. This period is significantly smaller than that for bulk PPLN devices (>20 μm). In order to prevent the domain walls from merging together in the presence of short poling period, a small electrodes spacing of 20 μm is used, with 30-μm-long electrode teeth and a 25% duty cycle. Under these conditions, we have achieved a poling period as short as 2.4 μm and are only limited by the minimum feature size (600 nm) of our lithography. We believe that switching to deep ultraviolet or e-beam lithography can help us reach the submicrometer period.

The electric field needed for thin-film poling is found to be higher than that for bulk poling. Indeed, domain inversion starts to occur with an electrical field greater than 30 kV/mm, while the threshold field for the bulk LN [6] is ~21 kV/mm. This increase of the threshold for poling can be attributed to the bonding interface between the thin-film LN and the SiO_2 buffer layer, which hinders the domain inversion. At the same time, a high electric field is helpful to improve the poling yield, but it also speeds up the spread of the domain wall. Therefore, a trade-off should be found for the value of the field to be applied for actual poling.
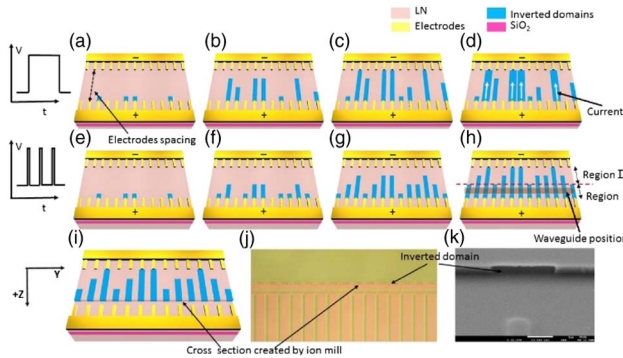

Fig. 1. Processing flow: (a) x-cut LN on insulator (LNOI) on an LN substrate; (b) electrode deposition; (c) surface poling of the LN thin film; (d) electrode removal and SiN deposition; and (e) SiN etching to form a ridge waveguide; (f) SiO_2 top cladding deposition.

Fig. 3. (a)–(d) Schematic illustration of the evolution of inverted domain using a long poling pulse. (e)–(h) Schematic illustration of the evolution of inverted domains using multi-pulse waveforms with short pulse durations. (i) Schematic of cross section of the device obtained after ion milling to visualize the periodically poled region. (j) Top-view micrograph of the cross section of a poled device after 10 min 48% HF etch at room temperature. The dashed line corresponds to the cross section in which the bright part is the poled area. (k) SEM image of inverted domain.

As schematically illustrated in Figs. 3(a)–3(d), the thin-film LN poling may suffer from low yield and bad uniformity using traditional long-pulse poling. This is due to severe random domain growth and domain wall spread from the heating of the current channel [18]. To mitigate it, a multi-pulse voltage waveform with a short pulse duration (∼10 ms) is applied. We notice that most of the nucleation sites where domain inversion starts from are generated at the beginning of a poling voltage pulse. Repeating the pulses thus allows the generation of more nucleation sites. This helps improve the uniformity of domain growth. The short pulse terminates before the temperature rises, thus minimizing the domain wall spread. Figures 3(e)–3(h) show the schematic evolution of the inverted domain using this method.

To further improve the poling quality of the device, the waveguide location is carefully designed. It was found that the best poling profile is achieved if the waveguide is defined closer to the positive electrode, shown in Fig. 3(h). The width of this region [labeled "Region I" in Fig. 3(h)] increases with the number of poling pulses, which should be set high enough to yield a large number of nucleation sites. However, too many pulses may also increase the leakage current, spread, or even merge the inverted domain and destroy the uniformity of the duty cycle. In this work, the poling conditions are optimized so that the width of Region I is ∼4 µm. This allows the waveguide mode to fully overlap with the inverted domains without significantly influencing the duty cycle's uniformity. In order to reveal the inverted domain, we use ion milling to create a cross section and let the z-surface of the crystal be exposed. By using hydrofluoric (HF) etching, which attacks inverted and non-inverted domains differently, the poling position can be visualized. Figure 3(j) shows the poling profiles in Region I for the actual device, which has 100% yield and good duty cycle uniformity. Figure 3(k) shows a zoomed-in picture of the inverted domain under a scanning electron microscope (SEM). The etched thickness by ion milling is 500 nm, and the poling profile fully penetrated this thickness with an almost-constant duty cycle.

In this work, we chose a relatively high electric field (48 kV/mm) to improve the poling yield. A pulse duration of 10 ms leads to a good poling profile. We used 2 pulses, resulting in a duty

cycle of $(40 \pm 10)\%$ and an almost 100% yield. The interval between two pulses is 10 s to reduce thermal issues. These conditions resulted in a poling quality that is comparable to bulk LN poling [24].

3. RESULTS AND DISCUSSION

The performances of the PPLN are evaluated in terms of SHG. A tunable single-frequency CW laser (Agilent 81642A, typical linewidth: ∼0.1 MHz, spectral range: 1510–1640 nm) is used as the seed. An erbium-doped fiber amplifier (IPG EAR-2K-C) is used during high-power testing. Light is passed through a polarization controller to excite the TE-polarized mode of the waveguide. Tapered lensed fibers couple the light in and out of the PPLN device. A wavelength-division multiplexer is placed at the output to split the pump light and the SH light. A telecom-wavelength optical power meter and an Si-PIN photo-detector are used to monitor the pump and SH power, respectively. Finally, the output spectra are recorded by an optical spectrum analyzer (Yokogawa AQ6370C).

The propagation loss of the waveguide was measured to be $\alpha_\omega \cong (0.3 \pm 0.2)$ dB/cm around 1550 nm. This is a record low value for a heterogeneous LN waveguide. The ultra-low loss of this device is comparable with the best results of the proton exchange and Ti in-diffused waveguides [10], which is essential for building long PPLN devices. The loss increases to ∼1 dB/cm around 1530 nm, which may be attributed to N–H bonds in the SiN.

The normalized SHG efficiency for a device with a 6.6 µm period is shown in Fig. 4(a). The peak normalized efficiency $\eta_{\rm nor}$ we achieved is ∼160% $W^{-1} \cdot cm^{-2}$ at a 1530 nm pumping
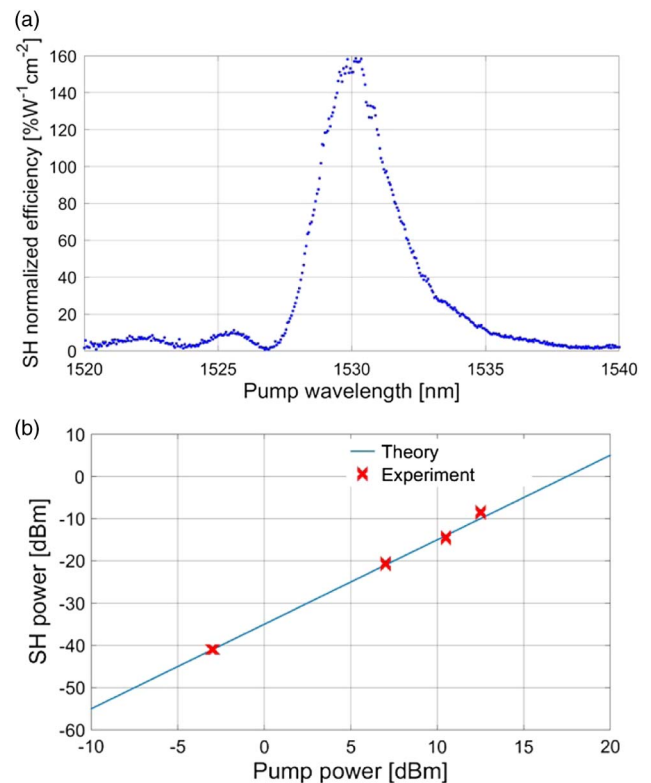

Fig. 4. PPLN waveguide characterized as a wavelength converter using SHG: (a) normalized efficiency as a function of the pump wavelength; and (b) peak generated SH power under different pump powers (red crosses), compared to theoretical predictions from (S7), assuming $\eta_{\rm nor} = 160\%$ $W^{-1} \cdot cm^{-2}$.

wavelength. This is more than 4 times larger than that of typical PPLNs (30%–40% $W^{-1} \cdot cm^{-2}$) [6]. The SH power generated is 80 nW at a pump power of 0.5 mW. Figure 4(b) shows the peak SH power under different pump powers. A good agreement is obtained with the theoretical predictions, assuming $\eta_{nor} = 160\%$ $W^{-1} \cdot cm^{-2}$. The coupling loss at the telecom band is ~6 dB per facet. For SH light, the coupling loss plus the propagation loss in the lensed fiber is ~14 dB. The relative high insertion losses at the input and output are mainly due to the much smaller mode size and to the fact that lensed fibers are multi-mode for SH light, which increases both the coupling and propagation loss of the fiber. This influences the external conversion efficiency. However, adding waveguide tapers at both the input and output to match the spot size can help reduce the coupling losses. Moreover, switching to free-space coupling may also reduce the loss caused by the lensed fiber, in particular for the SH light. We would expect that finally, the coupling loss is comparable to bulk PPLN waveguides.

The 3 dB bandwidth of the actual normalized efficiency for the pump light is around 3 nm, which is three times wider than the theoretical prediction (~1 nm). However, the actual normalized efficiency is ~10 times lower than the simulated value (1600% $W^{-1} \cdot cm^{-2}$). The imperfect duty cycle and its non-uniformity cause an efficiency drop of 30%, according to [25]. This assumes the duty cycle is normally distributed with an expectation of $\mu = \Lambda \cdot 40\%$ and a standard deviation of $\sigma = \Lambda \cdot 10\%$, where Λ is the poling period. Another reason for the discrepancy may be due to the waveguide non-uniformity, especially the non-uniform LN thickness (see Supplement 1). Further optimizing of the poling conditions can result in a duty cycle closer to 50% with better uniformity. The fabrication procedures can also be optimized to improve the waveguide uniformity. By carefully selecting the sample position on the wafer, the LN thickness variation can be controlled within 1 nm over a length of 1 cm. We thus expect to fabricate devices with even better performances after solving these problems.

4. CONCLUSION

We have demonstrated the first integration-compatible PPLN wavelength converter on a submicrometer LN film. The novel waveguide and poling technologies not only enhance the nonlinear conversion efficiency, but also enable photonic integration with different material systems. The device shows a peak normalized efficiency of 160% $W^{-1} \cdot cm^{-2}$ at 1530 nm for SHG, with 0.3 dB/cm waveguide propagation loss at the telecom band. The normalized efficiency of the device can be improved by an extra order of magnitude with optimized fabrication. We believe that this approach is a key technology for the integration of QPM devices with record-high efficiency in various chip-level microsystems as functional devices.

See Supplement 1 for supporting content.

REFERENCES

1. L. K. Oxenløwe, F. Gomez Agis, C. Ware, S. Kurimura, H. C. H. Mulvad, M. Galili, K. Kitamura, H. Nakajima, J. Ichikawa, D. Erasme, A. T. Clausen, and P. Jeppesen, "640 Gbit/s clock recovery using periodically poled lithium niobate," Electron. Lett. **44**, 370–371 (2008).
2. E. Saglamyurek, J. Jin, V. B. Verma, M. D. Shaw, F. Marsili, S. W. Nam, D. Oblak, and W. Tittel, "Quantum storage of entangled telecom-wavelength photons in an erbium-doped optical fibre," Nat. Photonics **9**, 83–87 (2015).
3. J. D. Jost, T. Herr, C. Lecaplain, V. Brasch, M. H. P. Pfeiffer, and T. J. Kippenberg, "Counting the cycles of light using a self-referenced optical microresonator," Optica **2**, 706–711 (2015).
4. S. Koke, C. Grebing, H. Frei, A. Anderson, A. Assion, and G. Steinmeyer, "Direct frequency comb synthesis with arbitrary offset and shot-noise-limited phase noise," Nat. Photonics **4**, 462–465 (2010).
5. F. Généreux, C. Baldenberger, B. Bourliaguet, and R. Vallée, "Low-voltage tunable second-harmonic generation in an x-cut periodically poled lithium niobate waveguide," Opt. Lett. **32**, 1108–1110 (2007).
6. L. Gui, "Periodically poled ridge waveguides and photonic wires in LiNbO₃ for efficient nonlinear interactions," Ph.D. thesis (University of Paderborn, 2010).
7. S. P. Kuo, J. Bravo-Abad, and G. S. Solomon, "Second-harmonic generation using 4-quasi-phase matching in a GaAs whispering-gallery-mode microcavity," Nat. Commun. **5**, 3109 (2014).
8. N. Segal, S. Keren-Zur, N. Hendler, and T. Ellenbogen, "Controlling light with metamaterial-based nonlinear photonic crystals," Nat. Photonics **9**, 180–184 (2015).
9. R. W. Boyd, *Nonlinear Optics*, 3rd ed. (Academic, 2008).
10. K. R. Parameswaran, R. K. Route, J. R. Kurz, R. V. Roussev, M. M. Fejer, and M. Fujimura, "Highly efficient second-harmonic generation in buried waveguides formed by annealed and reverse proton exchange in periodically poled lithium niobate," Opt. Lett. **27**, 179–181 (2002).
11. W. Jin and K. S. Chiang, "Mode switch based on electro-optic long-period waveguide grating in lithium niobate," Opt. Lett. **40**, 237–240 (2015).
12. R. Geiss, S. Saravi, A. Sergeyev, S. Diziain, F. Setzpfandt, F. Schrempel, R. Grange, E. B. Kley, A. Tünnermann, and T. Pertsch, "Fabrication of nanoscale lithium niobate waveguides for second-harmonic generation," Opt. Lett. **40**, 2715–2718 (2015).
13. R. Takigawa, E. Higurashi, T. Kawanishi, and T. Asano, "Lithium niobate ridged waveguides with smooth vertical sidewalls fabricated by an ultra-precision cutting method," Opt. Express **22**, 27733–27738 (2014).
14. H. Hu, R. Ricken, and W. Sohler, "Lithium niobate photonic wires," Opt. Express **17**, 24261–24268 (2009).
15. S. Kurimura, Y. Kato, M. Maruyama, Y. Usui, and H. Nakajima, "Quasi-phase-matched adhered ridge waveguide in LiNbO₃," Appl. Phys. Lett. **89**, 191123 (2006).
16. K. Mizuuchi, K. Yamamoto, and M. Kato, "Harmonic blue light generation in X-cut MgO:LiNbO₃ waveguide," Elect. Lett. **33**, 806–807 (1997).
17. T. Sugita, K. Mizuuchi, Y. Kitaoka, and K. Yamamoto, "Ultraviolet light generation in a periodically poled MgO:LiNbO₃ waveguide," Jpn. J. Appl. Phys. **40**, 1751–1753 (2001).
18. K. Mizuuchi, A. Morikawa, T. Sugita, and K. Yamamoto, "Electric-field poling in Mg-doped LiNbO₃," J. Appl. Phys. **96**, 6585–6590 (2004).
19. J. Chiles and S. Fathpour, "Mid-infrared integrated waveguide modulators based on silicon-on-lithium-niobate photonics," Optica **1**, 350–355 (2014).
20. L. Chen, A. Xu, M. G. Wood, and R. M. Reano, "Hybrid silicon and lithium niobate electro-optical ring modulator," Optica **1**, 112–118 (2014).
21. P. Rabiei, J. Ma, S. Khan, J. Chiles, and S. Fathpour, "Heterogeneous lithium niobate photonics on silicon substrates," Opt. Express **21**, 25573–25581 (2013).
22. L. Chen and R. M. Reano, "Compact electric field sensors based on indirect bonding of lithium niobate to silicon microrings," Opt. Express **20**, 4032–4038 (2012).

23. www.photond.com.
24. G. D. Miller, "Periodically poled lithium niobate: modelling, fabrication, and nonlinear-optical performance," Ph.D. thesis (Stanford University, 1998).
25. S. Helmfrid and G. Arvidsson, "Influence of randomly varying domain lengths and nonuniform effective index on second-harmonic generation in quasi-phase-matching waveguides," J. Opt. Soc. Am. B **8**, 797–804 (1991).